Available online at www.sciencedirect.com
ScienceDirect
International Journal of Heat and Mass Transfer 51 (2008) 3399–3409
International Journal of HEAT and MASS TRANSFER
www.elsevier.com/locate/ijhmt

An explicit–implicit time stepping scheme for solidification models

R. Pardeshi [a], V.R. Voller [b], A.K. Singh [a], P. Dutta [c,*]

[a] Tata Research Development and Design Centre, 54 B Hadapsar Industrial Estate, Pune 411 013, India
[b] Department of Civil Engineering, University of Minnesota, Minneapolis, MN 55455, USA
[c] Department of Mechanical Engineering, Indian Institute of Science, Bangalore 560 012, India

Received 29 June 2007; received in revised form 3 November 2007
Available online 22 April 2008

Abstract

A numerical scheme with hybrid explicit and implicit time stepping in solidification problems is presented. An explicit time stepping scheme is used for solving coupled temperature and concentration fields, while an implicit scheme is used for solving equations of motion. The explicit approach results in a local point-by-point coupling scheme for the temperature and concentration fields that uses constitutive model for back diffusion in solid. The present method offers distinct advantages of simplicity and flexibility in incorporation of micro-scale models, as demonstrated by the use of a back diffusion parameter in the microsegregation model. Results from the present method are compared with those in the literature using a fully implicit method, and they show significant improvement in final macrosegregation prediction.

Keywords: Solidification; Macroscopic model; Explicit; Macrosegregation; Back diffusion

1. Introduction

Solidification of binary mixtures does not exhibit a distinct front separating solid and liquid phases. Instead, the solid is formed as a permeable, fluid saturated, crystalline-like matrix. The structure and extent of this multiphase region, known as the mushy region, depends on numerous factors, such as the specific boundary and initial conditions. During solidification, latent energy is released at the interfaces which separate the phases within the mushy region. The distribution of this energy therefore depends on the specific structure of the multiphase region. Latent energy released during solidification is transferred by conduction in the solid phase, as well as by the combined effects of conduction and advection in the liquid phase. Fluid motion may be induced by external means, may occur naturally by thermal and/or solutal buoyancy forces, and may also be caused by expansion or contraction of the system due to the phase transformation. Concentration variations are primarily due to differences in the solubilities of constituents within each phase. Such differences lead to the selective rejection of constituents at microscopic phase interfaces. The rejected constituents are transported by fluid advection and, to a lesser extent, by diffusion within the phases.

A general solidification system, as seen in Fig. 1, involves a solid region, a liquid region and a mushy region. Often, the scale required for the resolution of the solid–liquid interface in the mushy region is several orders of magnitude smaller than the typical cell size used in a discrete numerical solution of the governing macroscopic transport equations. The concept of representative volume element (REV) was introduced by Ni and Beckermann [1]. Typically a REV is selected to include a representative and uniform sampling of the mushy region such that local scale solidification processes can be described by variables averaged over the REV.

The combination of the macroscopic transport equations and the specification of the nature of the REV can be used to provide a description of a given solidification system. Fig. 1 illustrates a general alloy system solidifying

* Corresponding author. Tel.: +91 80 2293 3225; fax: +91 80 2360 4536.
E-mail address: pradip@mecheng.iisc.ernet.in (P. Dutta).

0017-9310/$ - see front matter © 2008 Elsevier Ltd. All rights reserved.
doi:10.1016/j.ijheatmasstransfer.2007.11.060

Nomenclature

A	permeability constant
a	control volume face area (m^2)
C	solute concentration (wt%)
c	specific heat (J/kg K)
D	mass diffusivity (m^2/s)
F	flux at control volume face
f	mass fraction
g	liquid fraction
gr	gravity acceleration (m^2/s)
h	enthalpy (J/kg)
m	slope of the liquidus line
K	thermal conductivity (W/m K)
k_0	permeability constant
p	pressure (Pa)
S	source term
T	temperature (K)
t	time (s)
U	velocity (m/s)

Greek symbols

α	diffusion parameter
β	back diffusion parameter
β_T	thermal expansion coefficient (1/K)
β_c	solutal expansion coefficient
ρ	density (kg/m^3)
ρC	mixture concentration
ρH	mixture enthalpy
Φ	variable
Γ	diffusion constant
ΔH	latent heat (J/kg)
Δt	time step (s)
Δx	control volume length in x-direction (m)
Δy	control volume length in y-direction (m)
λ	secondary dendrite arm spacing (m)

Subscripts

s	solid
l	liquid
T	thermal
C	solutal
eut	eutectic
f	fusion
i	grid number in x-direction
j	grid number in y-direction
old	previous time step value
max	maximum value
n	north face of control volume
s	south face of control volume
e	east face of control volume
w	west face of control volume

Superscripts

ref	reference value
k	kth phase
s	solid phase
n	time level

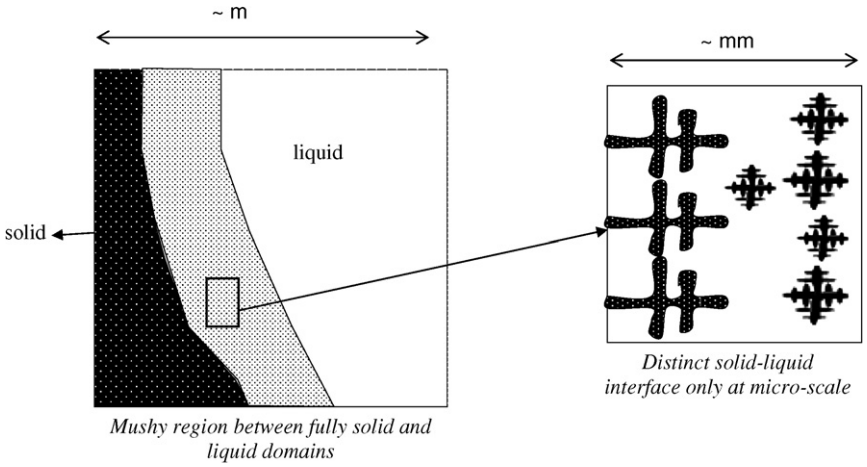

Fig. 1. A general solidification system.

in a two-dimensional domain. The material in the domain is initially liquid. Solidification is initiated on cooling the left wall. The remaining sides of the domain are insulated. During solidification, three distinct phases can co-exist, fully solidified region, mushy region and liquid region. From the momentum transport point of view, the presence of solid in the mushy region acts as drag on flow. Physically, the mushy region is a mixture of solid and liquid. The flow in the mush can be estimated in two ways. The mushy region can be treated as a porous media where the solid is stationary and the liquid flows through the porous structure [5]. This treatment is valid when solidification

progresses in columnar fashion. Alternatively, the mush can be considered as a mixture of solid crystals and liquid. In this case the movement of both the solid and liquid is permitted and this representation is closer to the equiaxed mode of solidification. These two physical situations represent two extremes. In many cases, however, solidification takes place through columnar as well as equiaxed, i.e. by columnar mode in the beginning of solidification and by equiaxed mode in later period. In such cases, a morphological transition from columnar to equiaxed takes place during the course of solidification. Therefore, a true representation of mushy phase can be through a combination of Darcy's law and variable viscosity formulation. Such representation would also require a criterion for columnar-to-equiaxed transition (CET) under transient convection which is not readily available. Additionally, at high solid fractions the equiaxed grains consolidate and solid phase can be treated as stationary with respect to mould. Fully solidified region, columnar structure of the mushy region, and consolidated equiaxed zone will move with a prescribed velocity ($\mathbf{U}_s$) if the casting is moving with respect to inertial frame of reference.

The driving force for the flow in liquid and mushy region can be thermal and solutal buoyancy, shrinkage and forced convection. From the above discussion, it is apparent that during equiaxed solidification, solid grains in the mushy region can have independent velocity specially at low solid fraction and this requires the specification of an equation of motion for its resolution [2]. An important consequence of the flow of solid and liquid in the mushy region is the large-scale transport of the solute components and as a result – in addition to solute variations over the sub-REV (microsegregation) – the solute varies over the domain as a whole (macrosegregation).

A key part in modeling the general system shown in Fig. 1 is the coupling between the temperature and concentration fields [3–13]. The main variables describing these fields are found by solving conservation equations on the macroscale of the REV. A complete resolution, however, requires a coupling between the solid fraction, liquid and solid concentrations, and temperature at the sub-REV scale (local scale) of the dendritic arm spaces. Voller et al. [14,15] have developed a general numerical approach for coupling the temperature and concentration fields which is different from many of the previous schemes [3–13]. In this approach, an explicit time stepping scheme is used to solve the thermal and concentration conservation equations. The disadvantage of this approach is a small time step for stability but it is offset by a straightforward numerical scheme that can readily incorporate multi-scale behavior. The incorporation into the solution algorithm of local scale microsegregation models that can accurately account for both back diffusion and coarsening effects was also demonstrated in a one-dimensional problem involving the solidification of a binary alloy from below [15]. In such a test geometry, if the rejected solute is lighter than the solvent, one-dimensional flow, downward towards the chill, is induced by solidification shrinkage. Accounting for this flow is straightforward requiring the satisfaction of the mass conservation. To date the explicit time stepping temperature–concentration coupling of Voller and co-workers [14] has not been tested in a multi-dimensional geometry, e.g. a binary alloy in a 2D cavity solidified from a vertical side. In this case, as noted above, the resulting fluid flow can be complex and its resolution will require the coupled solution of the momentum and mass conservation equations. The present approach, however, is different from some other approaches reported in the literature pertaining to incorporation of microscale issues in a macroscopic framework. For example, in Chakraborty and Dutta [16], a modified partition coefficient has been used to account solutal undercooling near the solid–liquid interface. Some other interesting studies on modeling microscale issues in a macroscopic framework are reported in [17–20].

The objective of the current work is to investigate the operation of the explicit time stepping temperature–concentration coupling algorithm in the simulation of a side cooled solidification of a binary-eutectic alloy in a two-dimensional cavity. In this effort a hybrid approach is used. The thermal and concentration fields are calculated with an explicit time stepping and their coupling achieved through the temperature–concentration algorithm similar to the one proposed by Voller et al. [14]. On the other hand, the flow field is solved with a fully implicit time stepping employing the well-known SIMPLER scheme for the velocity pressure coupling. The performance of this hybrid scheme is compared with that of a solution employing fully implicit time stepping in the solution of all fields. In addition the flexibility of the hybrid scheme to readily account for microsegregation and back diffusion is investigated in the context of published experimental data [21].

2. Governing equations

Using a volume-averaging technique, the general form of conservation of any scalar variable ϕ for each individual phase 'k' can be written as [1]:

$$\frac{\partial}{\partial t}(\rho_k g_k \phi_k) + \nabla \cdot (\rho_k g_k \vec{u}_k \phi_k) = \nabla \cdot (g_k \Gamma_k \nabla \phi_k) + g_k S_k \qquad (1)$$

where g_k is the volume fraction of the phase k, Γ_k is the corresponding diffusion coefficient, and S_k is a representative source term. Eq. (1) reduces to the form of well-known single-phase conservation equations, when summed over all the phases for the conservation of various quantities. For this purpose, the equivalent mixture density and velocity are defined as follows:

$$\rho = \sum_k \rho_k g_k, \quad \vec{u} = \sum_k \vec{u}_k f_k \qquad (2)$$

where f_k is the mass fraction of phase k.

If we make an extended Boussinesq approximation by neglecting solidification shrinkage, the equations of motion for the liquid phases for a fixed columnar microstructure

can be developed in terms of the interdendritic area averaged flow, $\mathbf{U}(U, V)$, as

$$\mathbf{U} = (1 - g_s)u_l, \tag{3}$$

where u_l is the actual fluid velocity.

The equation of continuity and motion for the interdendritic liquid velocity, $\mathbf{U}(U, V)$, can be written in the general form as follows:

Continuity:

$$\frac{\partial}{\partial t}(\rho) + \nabla \cdot (\rho_l \mathbf{U}) = 0 \tag{4}$$

U-momentum:

$$\frac{\partial}{\partial t}(\rho_l U) + \nabla \cdot (\rho_l \mathbf{U} U) = -\frac{\partial p}{\partial x} + \nabla \cdot [(1 - g_s)\mu \nabla U] - AU \tag{5}$$

V-momentum:

$$\frac{\partial}{\partial t}(\rho_l V) + \nabla \cdot (\rho_l \mathbf{U} V) = -\frac{\partial p}{\partial y} + \nabla \cdot [(1 - g_s)\mu \nabla V] - \rho_l(1 - g_s)\mathrm{gr} - AV \tag{6}$$

In the mushy region, additional source terms (last terms in Eqs. (5) and (6)) are there to account for the friction between liquid and solid fractions. The value of 'A' depends upon mush model used to represent porous media. In practice, the effect of the source term given by Eq. (6) is as follows. In fully liquid domain ($g_s = 0$), the source term is zero, and has no influence. In elements undergoing phase change, this term dominates over transient, convective and diffusive components of the momentum equation, thereby forcing them to imitate the porous media model. In fully solid elements ($g_s = 1$), however, an extremely large value of source term overweighs forces velocities to be zero. With the Boussinesq assumption invoked, the body force term in the y-momentum equation is modeled as

$$\rho_l \mathrm{gr} = \rho_l^{\mathrm{ref}} \mathrm{gr}(\beta_T(T - T^{\mathrm{ref}}) + \beta_c(C_l - C_l^{\mathrm{ref}})), \tag{7}$$

where ρ_l^{ref} is a constant reference density, β_T is thermal expansion coefficient, and β_c is the solutal expansion coefficient.

Mixture macroscopic conservation equations for heat and solute are derived similarly by adding the two-phase averaged equations. To begin with, we define the solid and liquid phase enthalpies as:

$$h_s = c_s T, \tag{8}$$

$$h_l = c_l T + \Delta H, \tag{9}$$

where c_s and c_l are the solid and liquid specific heats (assumed constant in respective phases), respectively. With the above definitions, the mixture enthalpy can be expressed as

$$[\rho \mathrm{H}] = g_s \rho_s h_s + (1 - g_s)\rho_l h_l \tag{10}$$

Neglecting dispersive fluxes, using Fourier's law and expanding the phase enthalpies in terms of temperature, the mixture energy conservation equation becomes

$$\frac{\partial[\rho \mathrm{H}]}{\partial t} + \nabla \cdot (\rho_l \mathbf{U} c_l T + \rho_l \mathbf{U} \Delta H) = \nabla \cdot [K \nabla T] \tag{11}$$

where K is a phase averaged conductivity. A linear variation of conductivity with volume fractions of individual phases is expressed as

$$K = g_s K_s + (1 - g_s)K_l \tag{12}$$

As diffusivities in liquid phase can be considered to be much higher than in solid phase, it may be reasonable to assume that the concentrations of the alloy components in the solid will be the only microscopic variables. Defining the concentration of the kth component in solid phase as C_s^k, the macroscopic solid concentration variable can be developed by performing volume averaging over the solid phase in the REV, i.e.

$$\langle C_s^k \rangle^s = \frac{1}{g_s} \int_0^{g_s} C_s^k \mathrm{d}\Gamma, \tag{13}$$

where $\mathrm{d}\Gamma$ is an elemental solid volume. Accordingly, the mixture concentration can be expressed as

$$[\rho \mathrm{C}]^k = g_s \rho_s \langle C_s^k \rangle^s + (1 - g_s)\rho_l C_l \tag{14}$$

Neglecting dispersive and macroscopic diffusion fluxes, the mixture solute conservation equation takes the following form

$$\frac{\partial[\rho \mathrm{C}]^k}{\partial t} + \nabla \cdot (\rho_l \mathbf{U} C_l^k) = 0 \tag{15}$$

3. Coupling relationships

Coupling relationship will be required to obtain solution for thermal and solute equations. In the present work, the coupling relationship formulated by Voller et al. [14] is used. The definitions of the mixture enthalpy $[\rho \mathrm{H}]$, and the mixture concentration $[\rho \mathrm{C}]$ gives two relationship equations. The third condition is obtained by imposing thermodynamic equilibrium at the solid–liquid interface, while the fourth relationship is obtained from the microsegregation model. The microsegregation model describes the local scale redistribution of solute in the REV. Following the definition of macroscopic solid concentration given in Eq. (13), the rate of change of a solute species in the solid fraction of the REV can be written as

$$\frac{\mathrm{d}[g_s \langle C_s \rangle^s]}{\mathrm{d}t} = k_{\mathrm{par}} C_l \frac{\mathrm{d}g_s}{\mathrm{d}t} + \int_0^{g_s} \frac{\partial C_s}{\partial t} \mathrm{d}\Gamma \tag{16}$$

On the right side of Eq. (16), the first term accounts for the partitioning of a solute species at the solid–liquid interface in the REV, while the second term accounts for the back diffusion of solute into the solid. The back diffusion term in Eq. (16) can be expressed more conveniently in an approximate form [22]:

$$\int_0^{g_s} \frac{\partial C_s}{\partial t} d\Gamma = \beta g_s k_{par} \frac{dC_l}{dt} \tag{17}$$

In this approximation, following the arguments laid out in [22], the β term can be modeled as

$$1 > \beta = \frac{8Dt_f g_s^{-4/3} + 0.2\lambda^2}{8Dt_f g_s^{-4/3} + 1.2\lambda^2} > 0 \tag{18}$$

where D is the solid diffusivity, λ is the secondary arm spacing and t_f is the solidification time; this model has been shown by Voller et al. [14,15] to provide an accurate description of microsegregation and coarsening processes, consistent with previous models in the literature. In this way Eq. (16) becomes

$$\frac{d[g_s \langle C_s \rangle^s]}{dt} = k_{par} C_l \frac{dg_s}{dt} + \beta g_s k_{par} \frac{dC_l}{dt} \tag{19}$$

where $0 < \beta < 1$ is a diffusion parameter accounting for back diffusion and arm coarsening in the REV. Note that the term β changes dynamically as the solidification evolves and in calculations estimates of t_f at a given point can be approximated from the solidification time of the nearest fully solid neighboring point (see [15]).

Another coupling relationship can be obtained from the equilibrium phase diagram:

$$T = G(C_l) \tag{20}$$

Thermodynamic equilibrium a solid–liquid interface also gives

$$C_s = k_{par} C_l \tag{21}$$

If we assume a linearized phase diagram of a binary-eutectic alloy, the temperature and liquid concentration are related through the liquidus line

$$T = T_f - mC_l \tag{22}$$

where T_f is the fusion temperature of the pure solvent and m is the slope of the liquidus line. The concentration in the primary solid phase, at the solid–liquid interface, is $C_s = k_{par} C_l$. When the eutectic concentration is reached, further solidification occurs isothermally at the eutectic temperature, $T = T_{eut}$.

4. Numerical details

In the present study, the temperature–concentration coupling used is similar to that described in Voller et al. [14]. For a full description of the algorithm one may refer to [14]. A flow chart of the algorithm is shown in Fig. 2. In present study, an equispaced structured grids is used. Initially [ρH] and [ρC] are solved using the explicit scheme. Subsequently, coupling equations are solved, undergoing inner iterations. Finally, flow equations are solved using an implicit scheme using the SIMPLER algorithm [23]. The discretized energy equation using an explicit time step scheme and finite difference method has the following form:

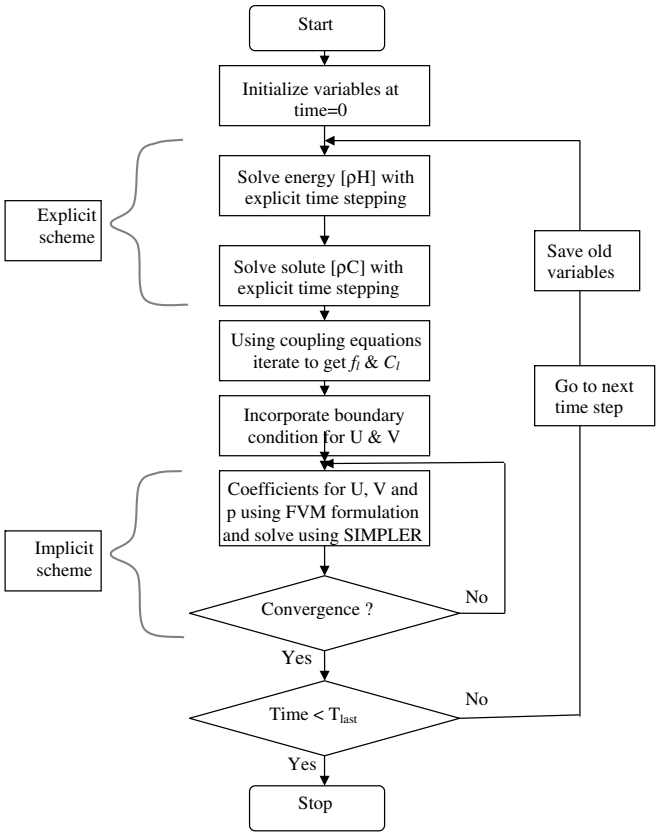

Fig. 2. Flow chart of the program.

$$\begin{aligned}
[\rho H]_{i,j}^{n+1} &= [\rho H]_{i,j}^{n} + \tfrac{\Delta t}{\Delta x^2} K(T_{i-1,j}^{n} - 2T_{i,j}^{n} + T_{i+1,j}^{n}) \\
&+ \tfrac{\Delta t}{\Delta y^2} K(T_{i,j-1}^{n} - 2T_{i,j}^{n} + T_{i,j+1}^{n}) \\
&- \tfrac{\Delta t}{\Delta x} c\{(T_{i,j}^{n} \| F_e, 0\| - T_{i+1,j}^{n} \| - F_e, 0\|) \\
&- (T_{i-1,j}^{n} \| F_w, 0\| - T_{i,j}^{n} \| - F_w, 0\|)\} \\
&- \tfrac{\Delta t}{\Delta y} c\{(T_{i,j}^{n} \| F_n, 0\| - T_{i,j+1}^{n} \| - F_n, 0\|) \\
&- (T_{i,j-1}^{n} \| F_s, 0\| - T_{i,j}^{n} \| - F_s, 0\|)\} \\
&- \tfrac{\Delta t}{\Delta x} \Delta H\{(\| F_e, 0\| - F_e, 0\|) \\
&- (\| F_w, 0\| - \| - F_w, 0\|)\} \\
&- \tfrac{\Delta t}{\Delta y} \Delta H\{(\| F_n, 0\| \| - F_n, 0\|) \\
&- (\| F_s, 0\| - \| - F_s, 0\|)\}
\end{aligned}$$

where, symbol $\| \ldots . \|$ represent maximum of two variables and $F_e = \rho_e a_e U_e$ is flux at east control volume face (flux equations at other control volume face have similar form).

Similarly, the discretized concentration equation has the following form:

$$\begin{aligned}
[\rho C]_{i,j}^{n+1} &= [\rho C]_{i,j}^{n} - \tfrac{\Delta t}{\Delta x}\{(C_{li,j}^{n} \| F_e, 0\| - C_{li+1,j}^{n} \| - F_e, 0\|) \\
&- (C_{li-1,j}^{n} \| F_w, 0\| - C_{li,j}^{n} \| - F_w, 0\|)\} \\
&- \tfrac{\Delta t}{\Delta y}\{(C_{li,j}^{n} \| F_n, 0\| - C_{li,j+1}^{n} \| - F_n, 0\|) \\
&- (C_{li,j-1}^{n} \| F_s, 0\| - C_{li,j}^{n} \| - F_s, 0\|)\}
\end{aligned}$$

The momentum (U, V) equations along with the continuity equation are discretized using a finite volume method (FVM) as described in Patankar [23]. These equations are

discretized using implicit time stepping scheme. The momentum and continuity equations are solved using SIMPLER algorithm [23] and tri-diagonal matrix solver. The convergence criteria for implicit iteration loop is when $|(\phi - \phi_{old})/\phi_{max}| < 10^{-5}$, where ϕ stands for solved variables at a grid point at the current iteration level, ϕ_{old} represents the corresponding value at the previous iteration level, and ϕ_{max} is the maximum value of the variable at the current iteration level in the entire domain. The convergence criteria for the iterative loop that solves the coupling equations is when the correction in the nodal solid fraction value satisfied the condition $|g - g_{old}| < 10^{-4}$ where g is solid fraction value at current iteration and g_{old} is solid fraction value at previous iteration.

5. Results and discussion

5.1. Numerical validation and parametric study

The test problem is taken from the existing literature [5]. We consider a two-dimensional rectangular cavity filled with a binary mixture (Fig. 3), which is initially liquid and uniform in temperature and composition. At time $t = 0$, the temperature of the left vertical boundary is instantaneously dropped and maintained at a temperature, T_{cold}, which is below the liquidus temperature, T_L. All other boundaries remain insulated. A zero mass flux condition prevails on all the walls of the cavity. The fluid flow is assumed to be laminar and unsteady. The binary fluid is considered to be Newtonian and incompressible, and its thermophysical data, given in Table 1, approximate those of aqueous ammonium chloride solution. The mushy region is modeled using Carman–Kozeny relations where parameter 'A' is defined as follows,

$$A = k_0 \frac{g_s^2}{(1 - g_s)^3}$$

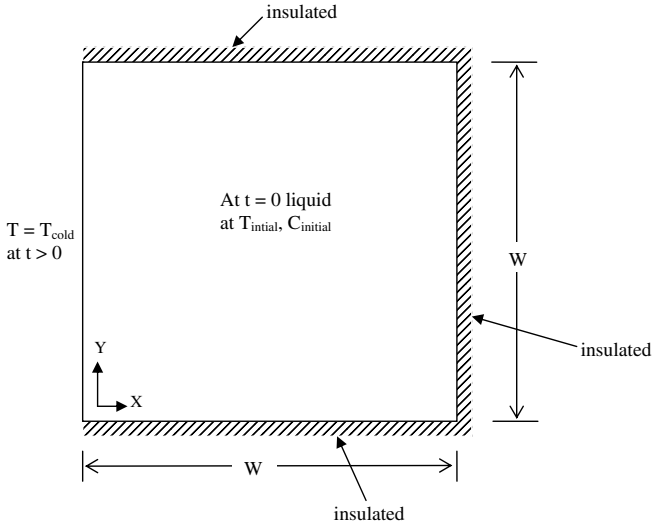

Fig. 3. Schematic sketch of the test problem.

Table 1
Process parameters and thermophysical properties of ammonium-chloride system

Initial and boundary conditions	
Cavity dimensions	$w = 0.025$ m
Initial liquid concentration	$C_{intial} = 0.1$ kg/m^3
Initial temperature	$T_{hot} = 600$ K
Left wall temperature for time > 0	$T_{cold} = 400$ K
Thermophysical properties	
Specific heat	$c_p = 3000$ J/kg K
Thermal conductivity	$K = 0.4$ W/m K
Density	$\rho = 1000$ kg/m^3
Liquid viscosity	$\mu = 1.0 \times 10^{-3}$ kg/m s
Species diffusion coefficient	$D = 4.8 \times 10^{-9}$ m^2/s
Latent heat	$H = 3 \times 10^5$ J/kg
Permeability coefficient	$k_0 = 2 \times 10^6$ kg/m^3 s
Thermal expansion coefficient	$\beta_T = 4 \times 10^{-5}$ K^{-1}
Solutal expansion coefficient	$\beta_s = 0.025$
Eutectic temperature	$T_{eut} = 250$ K
Eutectic concentration (mass fraction)	$C_{eut} = 0.8$
Melting point of pure material	$T_m = 630$ K
Equilibrium partition ratio	$k_{par} = 0.3$

With this condition, solidification of the alloy immediately commences at the cold boundary, and at a later times, three regions will exist in the cavity; a full solid region, a mushy region, and a full liquid region. The grid size used for simulation is 40×40 (same as reported in [5]) and time step used is 0.0025 s.

5.1.1. Evolution of double-diffusive convection and macrosegregation

Double diffusive convection will result in this case, as the flow will be influenced by temperature gradients (caused by the thermal boundary conditions) as well as solutal gradients (caused by solute rejection at the solid–liquid interface). The final pattern of macro-segregation will depend on the evolution of flow field during the solidification process. Thermally driven flow will dominate initially, as high temperature gradients exist and the fluid composition is uniform and close to the initial concentration. As solidification proceeds, however, the thermal gradients decay and solute concentration gradients build up. For studying the evolution of the flow field and its effect on macrosegregation, we take snap shots of the flow field at different time levels. Immediately after lowering the left wall temperature to T_{cold}, thermal gradients cause a strong counterclockwise flow field. Fig. 4 shows the streamline pattern at $t = 100$ s. At later times, however, the thermal gradients weaken considerably and solute gradients build up. An indication of this phenomenon appears in the streamline pattern at 250 s (Fig. 5), which shows a small recirculation cell in the opposite direction (clockwise) at the lower left corner of the cavity. This solutally driven recirculation cell results from the steep concentration gradients near the base of the cavity. With further progress in solidification, thermal buoyancy weakens and solutal effects begin to dominate, leading to a reversal of circulation pattern at $t = 500$ s, as shown in Fig. 6.

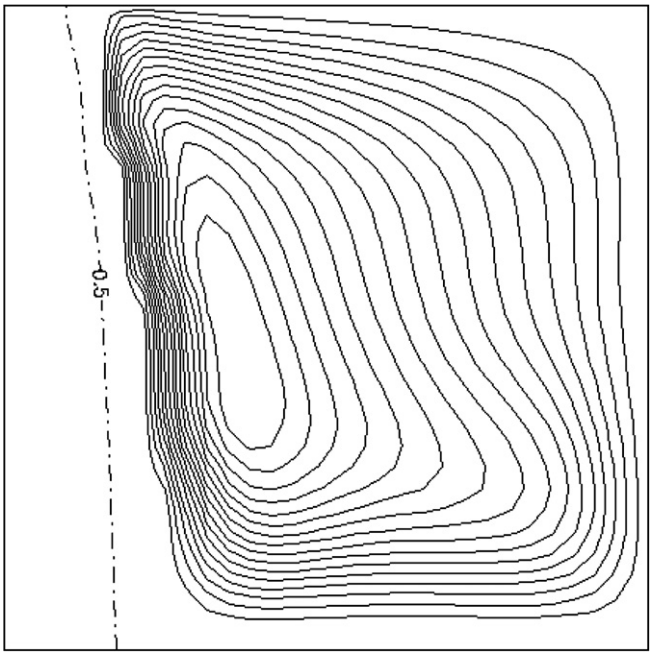

Fig. 4. Streamlines and solidification front at time = 100 s (maximum value = 0.0035118, minimum value = 0.0).

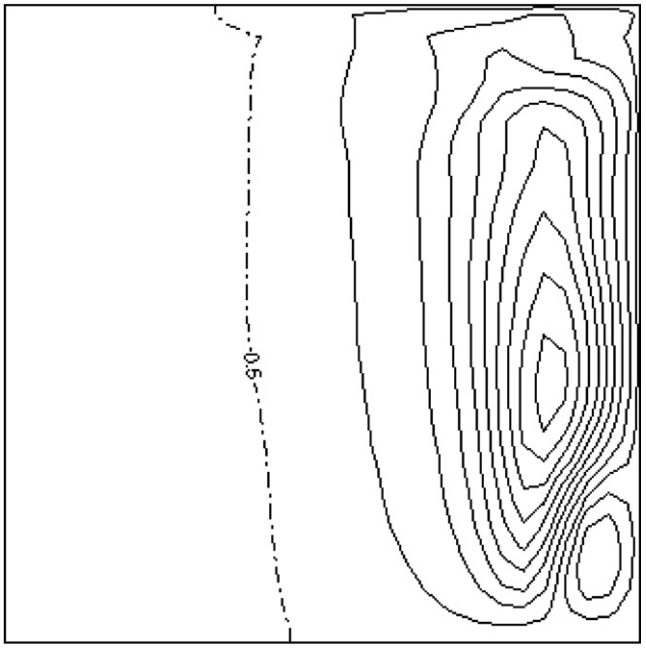

Fig. 6. Streamlines and solidification front at time = 500 s (maximum value = 5.63×10^{-5}, minimum value = -0.00018915).

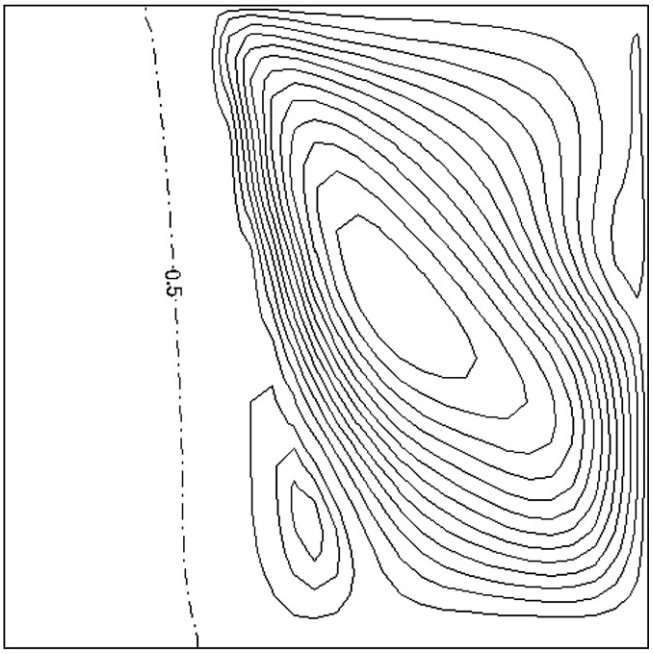

Fig. 5. Streamlines and solidification front at time = 250 s (maximum value = 0.0018846, minimum value = −0.00017434).

5.1.2. Comparison of present approach with existing fully implicit method

Fig. 7 shows macrosegregation pattern at the end of the solidification process. As observed in Fig. 7a, areas of positive segregation are located along the right of the upper portion of the cavity, which is caused by the solutally driven counter-clockwise circulation towards the later stages of solidification. Fig. 7b shows the corresponding results in the existing literature using a fully implicit method [5]. In order to benchmark the performance of the present method, we simulated the same test case using a fully implicit method with temperature–solute coupling modeled using the lever rule. Simulations were carried out on a machine with Pentium 4 (3.2 GHz, 1GB RAM) processor, with grid size and convergence criteria described in Section 4.

For simulation till time = 3000 s, fully implicit method took about 3 h run-time while explicit–implicit method took about 4 h run-time, where results by both methods show similar macrosegregation prediction. Hence, there is some but not a significant loss in efficiency in using the explicit temperature–concentration coupling. It needs to be emphasized, however, that the assumption of a Lever rule is a very basic means of accounting for the local scale (dendrite arm spacing) redistribution of solute. The proposed explicit concentration–temperature coupling is expected to prove to be an advantage when the microsegregation is more detailed, e.g. including such effects as back diffusion in to the solid phase.

5.1.3. Effect of back diffusion

A distinct feature of the present method is its local nature of the thermo-solutal coupling, and it offers advantages of simplicity and flexibility in moving towards more complex systems (i.e. incorporation of micro-scale models). The present explicit–implicit hybrid scheme can be used to make a quantitative assessment of the effect of back diffusion on macrosegregation predictions. Consider the system where segregation is due to thermo-solutal convection, as described in previous section. Comparison with the cases of no back diffusion $\beta = 0$ and complete

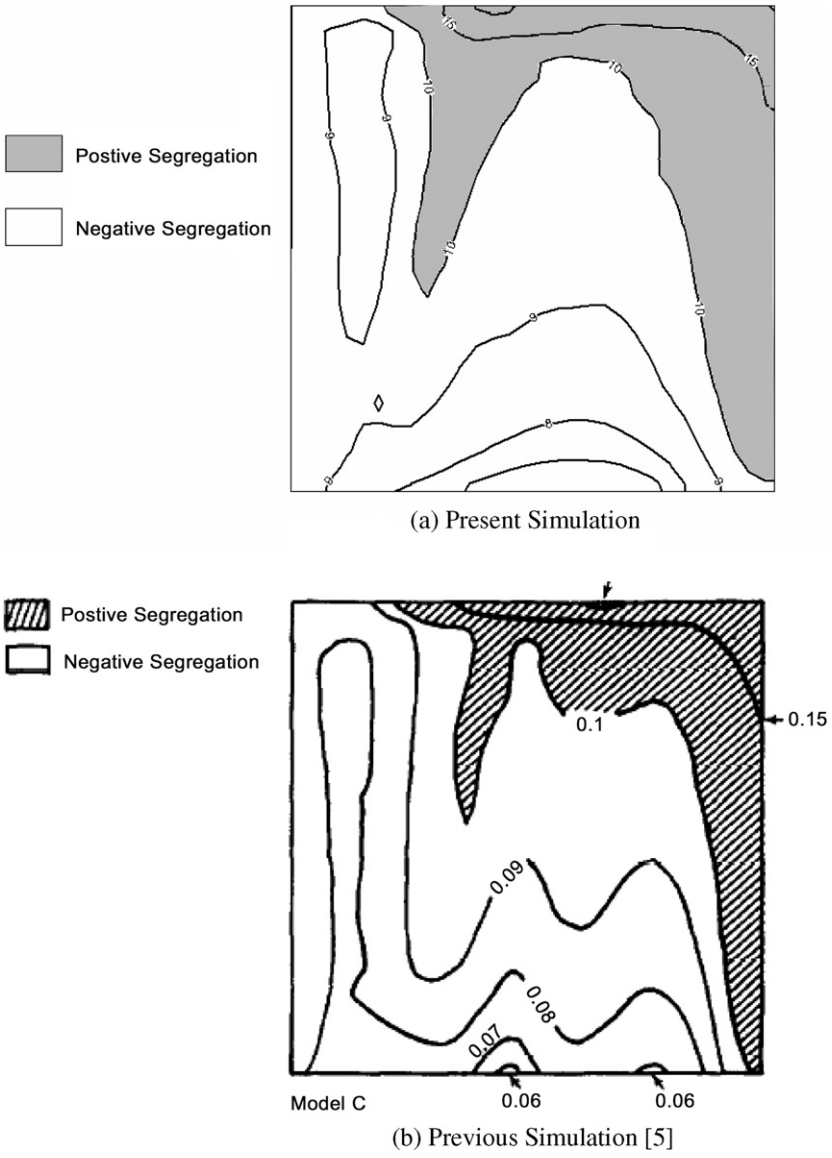

Fig. 7. Comparison of macrosegregation prediction with existing numerical simulation [5].

solid state diffusion $\beta = 1$ are shown in Fig. 8. Concentration profile at the end of solidification is shown along the vertical direction for $x = 0.06$ m. In case of back diffusion, solute diffusion occurs from solute rich liquid into the solidified region. This leads to transport of rejected solute from liquid into solid. Hence, the solute concentration is higher in the case where back diffusion is non-zero, except at the top portion of the cavity. At the top of the cavity, there is a larger positive segregation for this case (see Fig. 7), as more solute is available during the closing stages of solidification.

5.2. Case study: solidification of Pb–15wt%Sn in a square cavity

The model is subsequently used to simulate solidification of Pb–15wt%Sn alloy in a square cavity having dimensions 0.1 m × 0.1 m. The vertical boundaries are subjected to prescribed temperature conditions, and the horizontal boundaries are kept insulated. The melt, with an initial superheat, is poured into the cavity, where it starts solidifying from a vertical boundary. For this test case, experimental data is reported in literature [21] along with simulation results assuming Schiel model for microsegregation. The variations of boundary temperatures with time are shown in Fig. 9, in accordance with the experimental data reported in [21]. The relevant thermophysical properties of Pb–15wt%Sn alloy are listed in Table 2 [21]. The mushy region (parameter '*A*') is modeled using West permeability relations as reported in [21]. The grid size used for simulation is 40 × 40 (same as reported in [21]) and time step used is 0.0025 s.

5.2.1. Macrosegregation predictions

Since the cavity is side cooled, thermal buoyancy effects tend to push the fluid down the phase changing interface.

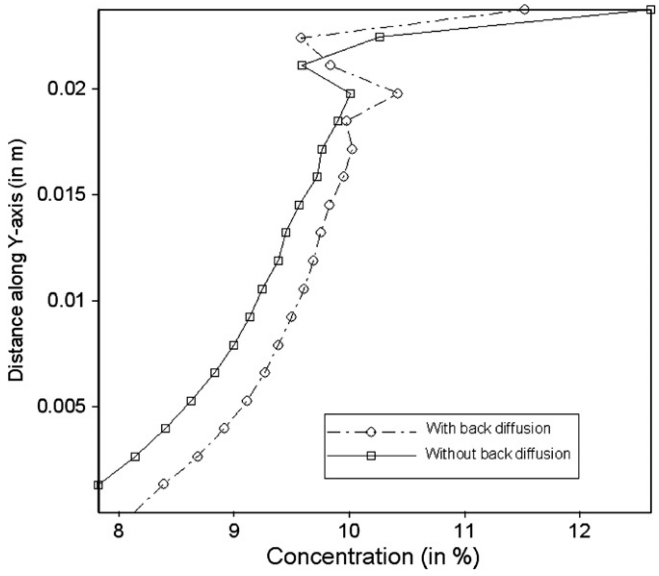

Fig. 8. Macrosegregation along y axis for $x = 19$ mm.

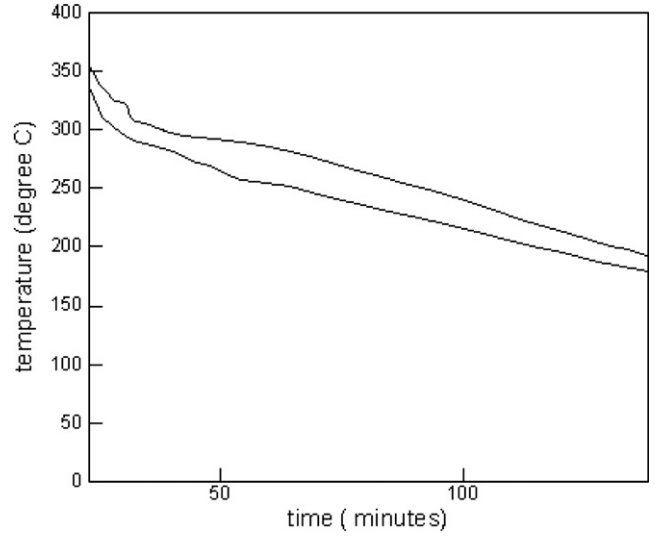

Fig. 9. Cavity left and right wall temperature measured by Shahani et. al. [21].

Table 2
Thermophysical properties of Pb–15wt%Sn

Specific heat (c)	154.6 J/kg
Thermal conductivity of solid (K_s)	34.97 W/m K
Thermal conductivity of liquid (K_l)	17.8 W/m K
Density (ρ)	10,100 kg/m^3
Viscosity (μ)	2.53×10^{-3} kg/m s
Liquid diffusion coefficient (D_l)	1×10^{-9} m^2/s
Latent heat of fusion (ΔH)	2.47×10^4 J/kg
Thermal expansion coefficient (β_T)	1.23×10^{-4} K^{-1}
Solutal expansion coefficient (β_S)	0.339
Eutectic temperature (T_{eut})	456.14 K
Eutectic concentration (C_{eut})	0.619
Equilibrium partition coefficient (k_{par})	0.31

This leads to the formation of a large vortex rotating in the clockwise direction at the initial stages of solidification. However, as solidification proceeds, Sn is rejected into the liquid, which is lighter than the solvent (Pb) and hence tends to move up. Hence, thermal and solutal buoyancy effects oppose each other for the nominal composition 15wt%Sn in the alloy. With further progress in solidification, solutal buoyancy effects gain prominence, as in the case of hypereutectic ammonium chloride solution discussed previously in this section.

Figs. 10–12 show the final macrosgregation profiles at different vertical sections of the cavity. The results obtained by the present model (using constitutive model for back diffusion) are compared with the experimental observations [21] and with the corresponding numerical results obtained using Schiel model for microsegration. From these figures it is evident that there is a positive macrosegregation at

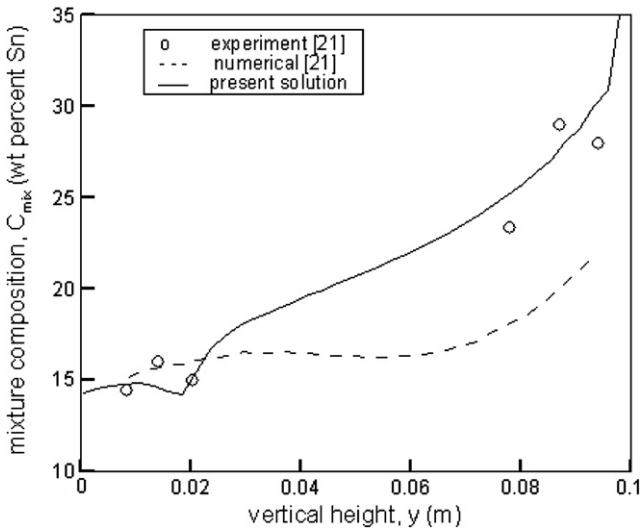

Fig. 10. Final macrosegregation for Pb–15wt%Sn alloy at $x = 9.47$ cm.

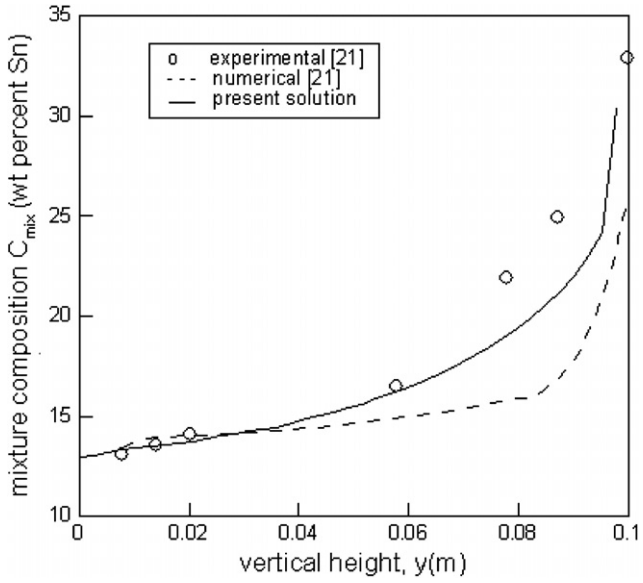

Fig. 11. Final macrosegregation for Pb–15wt%Sn alloy at $x = 8$ cm.

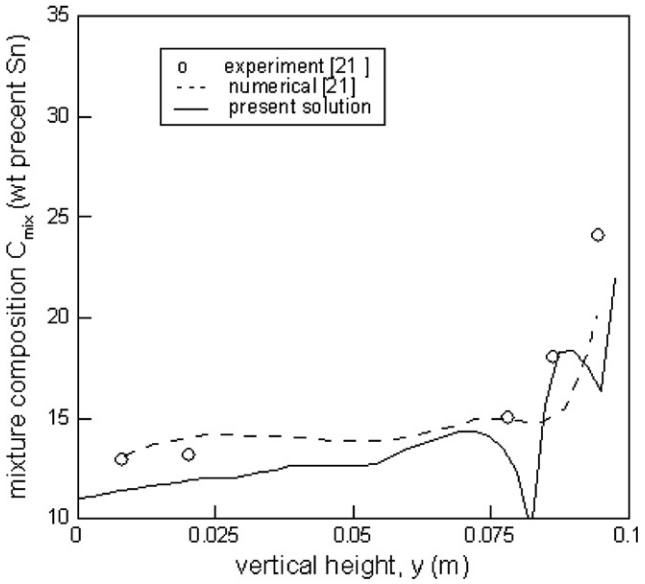

Fig. 12. Final macrosegregation for Pb–15wt%Sn alloy at $x = 3.5$ cm.

the top of the cavity, and negative macrosegregation in the rest of the cavity. Figs. 10 and 11 depict concentration variations along vertical lines located at $x = 9.47$ cm and $x = 8.0$ cm, respectively, corresponding to the region close to the right wall. Near the right wall, solidification commences from the bottom region and progresses towards the top, because of the nature of melt convection. As a result, it can be expected that the bottom region will have negative segregation and the top region will experience positive segregation. The negative segregation in the bottom region will be diminished by back diffusion effects, as observed in Figs. 10 and 11. The positive segregation in the upper region of the cavity is enhanced by the melt convection, which carries the excess solute in a clockwise direction to the top by thermal buoyancy. At later stages of solidification, however, the thermal buoyancy is opposed by solutal buoyancy. With back diffusion, the strength of solutal buoyancy is reduced, as there is less solute build-up at the interface. Hence, positive segregation at the top region of the cavity is under-predicted by Schiel's microsegregation model, as observed in Figs. 10 and 11. It is evident from the figures that the results obtained from the present numerical simulation incorporating constitutive model for back diffusion in solid are closer to the experimental results, as compared to the previous numerical simulation [21]. Fig. 12 shows macrosegregation pattern along a vertical line located at $x = 3.5$ cm. This line is closer to the left wall, and hence corresponds to a region experiencing solidification at an early stage. Although the trends predicted by the models agree with that of experiment, the model with back diffusion is found to under predict solid concentration near the bottom wall. At early stages of solidification, the region close to the left wall experiences solutal buoyancy forces opposing the downward thermally driven convection. This effect is more pronounced in the case of Schiel's model (without back diffusion), leading to more solute build-up at the interface and, consequently, higher concentration in the solid. A feature of the new results are the fluctuations near the top of the mold. The application of finer meshes of (72×72) and (120×120) gave similar results and indicated that the fluctuations could be attributed to the formation of "A" segregates.

6. Conclusion

In the present formulation, a numerical scheme with hybrid explicit and implicit time stepping in solidification problem is used. An explicit time stepping scheme is used for solving coupled temperature and concentration fields, with a coupling scheme for the temperature and concentration fields similar to that given in literature. After obtaining solution for temperature and concentration fields, the equations of motion are solved using a pressure based implicit method. Results from the present method compared well with those of a fully implicit method for the case of solidification in presence of double-diffusive convection in a square cavity. The flexibility of the present partial explicit scheme in incorporating complex microscale models is demonstrated by using a back diffusion parameter, and then numerically studying its effect on macrosegregation. Subsequently, the model is applied to the case of solidification of a Pb–Sn alloy in a square cavity. The simulation results are compared with the corresponding experimental results reported in the literature, and the present model shows significant improvement in macrosegregation predictions.

References

[1] J. Ni, C. Beckermann, A volume averaged two-phase model for transport phenomena during solidification, Metall. Trans. B 22 (1991) 349–361.
[2] C. Beckermann, C.Y. Wang, Multi-phase/-scale modeling of transport phenomena in alloy solidification, in: C.L. Tien (Ed.), Annual Review of Heat Transfer VI, Begell House, New York, 1995, pp. 115–198.
[3] W.D. Bennon, F.P. Incropera, The evolution of macro-segregation in statically cast binary ingots, Metall. Trans. B 18 (1987) 611–616.
[4] C. Beckermann, R. Viskanta, Double-diffusive convection during dendritic solidification of a binary mixture, Physico. Chem. Hydrodyn. 10 (1988) 195–213.
[5] V.R. Voller, A.D. Brent, C. Prakash, The modelling of heat mass and solute transport in solidification systems, Int. J. Heat Mass Transfer 32 (1989) 1719–1731.
[6] C.R. Swaminathan, V.R. Voller, Towards a general numerical scheme for solidification systems, Int. J. Heat Mass Transfer 40 (1997) 2859–2868.
[7] M.J.M. Krane, F.P. Incropera, D.R. Gaskell, Solution of ternary metal alloys – I. Model development, Int. J. Heat Mass Transfer 40 (1997) 3827–3835.
[8] M.C. Schneider, C. Beckermann, Formation of macrosegregation by multicomponent thermosolutal convection during solidification of steel, Metall. Trans. A 26 (1995) 2373–2388.
[9] S.D. Felicelli, J.C. Heinrich, D.R. Poirier, Simulation of freckles during vertical solidification of binary alloys, Metall. Trans. B 22 (1991) 847–859.

[10] G. Amberg, Computation of macrosegregation in an iron–carbon cast, Int. J. Heat Mass Transfer 34 (1991) 217–227.
[11] H. Combeau, J.-M. Drezet, A. Mo, M. Rappaz, Modeling of microsegregation in macrosegregation computations 27 (8) (1996) 2314–2327.
[12] E. Arquis, M. Rady, A fixed domain model for microsegregation during solidification of binary alloys, Heat Mass Transfer 41 (2005) 545–558.
[13] M. Rady, E. Arquis, A dual-scale coupled micro/macro segregation model for dendritic alloy solidification, Heat Mass Transfer 42 (2006) 1129–1141.
[14] V.R. Voller, A. Mouchmov, M. Cross, An explicit scheme for coupling temperature and concentration fields in solidification models, Appl. Math. Model. 28 (2004) 79–94.
[15] V.R. Voller, Numerical methods for phase-change problems, in: W.J. Minkowycz, E.M. Sparrow, J.Y. Murthy, (Eds.), Handbook of Numerical Heat Transfer, second ed., 2006 (Chapter 19).
[16] S. Chakraborty, P. Dutta, The effect of solutal undercooling on double-diffusive convection and macro-segregation during binary alloy solidification: a numerical investigation, Int. J. Numer. Meth. Fl. 38 (2002) 895–917.
[17] S. Chakraborty, P. Dutta, Effects of dendritic arm coarsening on macroscopic modelling of solidification of binary alloys, Mater. Sci. Technol. 17 (2001) 1531–1538.
[18] S. Chakraborty, P. Dutta, A generalized formulation for evaluation of latent heat functions in enthalpy-based macroscopic models for convection–diffusion phase change process, Metall. Mater. Trans. B 32B (2001) 562–564.
[19] S. Chakraborty, P. Dutta, Three dimensional double-diffusive convection and macrosegregation during non-equilibrium solidification of binary mixtures, Int. J. Heat Mass Transfer 46 (2003) 2115–2134.
[20] S. Chakraborty, N. Chakraborty, P. Kumar, P. Dutta, Studies on turbulent momentum heat and species, transport during binary alloy solidification in a top-cooled rectangular cavity, Int. J. Heat Mass Transfer 46 (2003) 1115–1137.
[21] H. Shahani, G. Amberg, H. Fredriksson, On the formation of macrosegregation in unidirectionally solidified Sn–Pb and Pb–Sn alloys, Metall. Trans. A 23A (1992) 2301–2311.
[22] V.R. Voller, A semi-analytical model of microsegregation in a binary alloy, J. Crystal Growth 197 (1999) 325–332.
[23] S.V. Patankar, Numerical Heat Transfer and Fluid Flow, Hemisphere, Washington, DC, 1980.